Supplementary information for "Estimating the Raman cross sections of single carbon nanotubes", by *Johanna E. Bohn, Pablo G. Etchegoin, Eric C. Le Ru, Rong Xiang, Shohei Chiashi, and Shigeo Maruyama*

SECTION S1: CALIBRATION METHOD: SCATTERING VOLUME CHARACTERIZATION AND APPARENT CROSS SECTION OF SILICON

Hereafter, we explain how an apparent Raman cross-section for the $303\,\mathrm{cm}^{-1}$ mode of Si was measured and then used to infer the nanotube Raman cross-sections from the previously published data in Ref. 1 at 785 nm. We start by discussing the scattering volume characterization, which is also needed for a direct measurement of the nanotube Raman cross-section at 633 nm as discussed in the main text.

Scattering volume characterization

It is easier (for experimental reasons) to start with a substance with known differential cross section that can be measured in a *volume* (typically a liquid or a gas) rather than on a surface. This is because it is easier in this former case to estimate the number of molecules contributing to the signal (given the density and molecular weight of the substance). Henceforth, this implies the previous knowledge and characterization of the scattering volume, which is shown for our $\times 100$ objective (air) in Figures S1 (at 785 nm) and S2 (at 633 nm).

The scattering volume characterization is done by measuring first the *beam waist* (w_0), using the confocal pinhole and relating this value to the actual waist of the beam on the image plane through the magnification of the collecting optics. This is schematically shown in Fig. S1(a). Furthermore, it is necessary to determine the *depth of focus* (H_{eff}) in the axial direction, shown in Fig. S1(b). The full characterization of the scattering volume has been described in detail in the supplementary information of Ref. 2 and, therefore, it will not be repeated here. We only concentrate on a summary of the results in the following points:

- From the data at 785 nm in Fig. S1(a) (using the nomenclature and methods of Ref. 2) we obtain $w_0 = 1.2\,\mu$m, while the profile in the axial direction in Fig. S1(b) gives the effective depth of focus of $H_{\mathrm{eff}} = 19\,\mu$m. From here we obtain an effective scattering volume of $V_{\mathrm{eff}}^{785\,\mathrm{nm}} = (\pi/2) w_0^2 H_{\mathrm{eff}} = 43.0\,\mu\mathrm{m}^3$ at 785 nm laser excitation with an effective spot area of $A_{\mathrm{eff}}^{785\,\mathrm{nm}} = 2.26\,\mu\mathrm{m}^2$.

- As a calibration Raman standard for differential cross sections, we use the nitrogen gas in air at normal atmospheric conditions. We can calculate the effective number of molecules (N) contained in the scattering volume from the partial pressure of nitrogen (78%): $N = 8.1\,10^8$ molecules.

- With N known, we can take the differential Raman cross section per molecule of N_2 (for the only vibration at $2331\,\mathrm{cm}^{-1}$, with $d\sigma/d\Omega = 7 \times 10^{-32}\,\mathrm{cm}^2/\mathrm{sr}$ at 785 nm) and write down an expression for the signal measured by the spectrometer as:

$$I_{\mathrm{N_2}} = \alpha \rho \tau N \cdot \left(\frac{d\sigma}{d\Omega}\right)_{\mathrm{N_2}}^{785\,\mathrm{nm}}, \qquad \text{(S1)}$$

  where the signal $I_{\mathrm{N_2}}$ is measured in counts, ρ is the power density [W/m^2], τ [sec] the integration time, and α is a fixed factor accounting for the overall collection efficiency. The actual signal of N_2 under the experimental conditions we are using ($650\,\mu$W @ 785 nm, 300 sec integration time, $\times 100$ objective) is shown explicitly in Fig. S1(c).

A similar characterization is carried out at 633 nm for the direct measurement of single nanotube cross-sections. The beam-waist (w_0) measurement (in Fig. S2(a)) with the confocal pinhole of our microscope rendered a value of $w_0 = 450$ nm, which combined with the axial effective depth of focus [2] of $H_{\mathrm{eff}} = 16.5\,\mu$m (in Fig. S2(b)) gives an effective scattering volume of $V_{\mathrm{eff}} = 5.25\,\mu\mathrm{m}^3$. For air at normal pressure and temperature this results in $N \approx 10^8$ nitrogen molecules contributing to the Raman signal. The differential Raman cross-section of N_2 at 633 nm is $(d\sigma/d\Omega)_{\mathrm{N_2}}^{633\,\mathrm{nm}} = 16 \times 10^{-32}\,\mathrm{cm}^2/\mathrm{sr}$ [3] (note that the cross section of N_2 changes with excitation wavelength due to the well known ω^4-dependence of cross sections for non-resonant molecules). We conclude that the peak in Fig. S2(c) (obtained with 300 sec integration time) is equivalent to an effective differential cross section of: $(d\sigma/d\Omega)_{\mathrm{N_2}}^{\mathrm{eff}} = N \times (d\sigma/d\Omega)_{\mathrm{N_2}}^{633\,\mathrm{nm}} = 1.6 \times 10^{-23}\,\mathrm{cm}^2/\mathrm{sr}$.

Finally, in order to use this calibration to determine the RBM's Raman cross-sections, we also need to correct for the difference in the system response between $2331\,\mathrm{cm}^{-1}$ (nitrogen) and $\sim 200\,\mathrm{cm}^{-1}$ (RBM's) at 633 nm excitation. This difference in response is a factor of 1.45 in our system (measured again against a calibrated lamp).

Apparent Si cross-section

Once the scattering volume has been fully characterized, an apparent Si cross-section can be defined and determined as follows. Under the same experimental conditions (power, integration time, numerical aperture of the

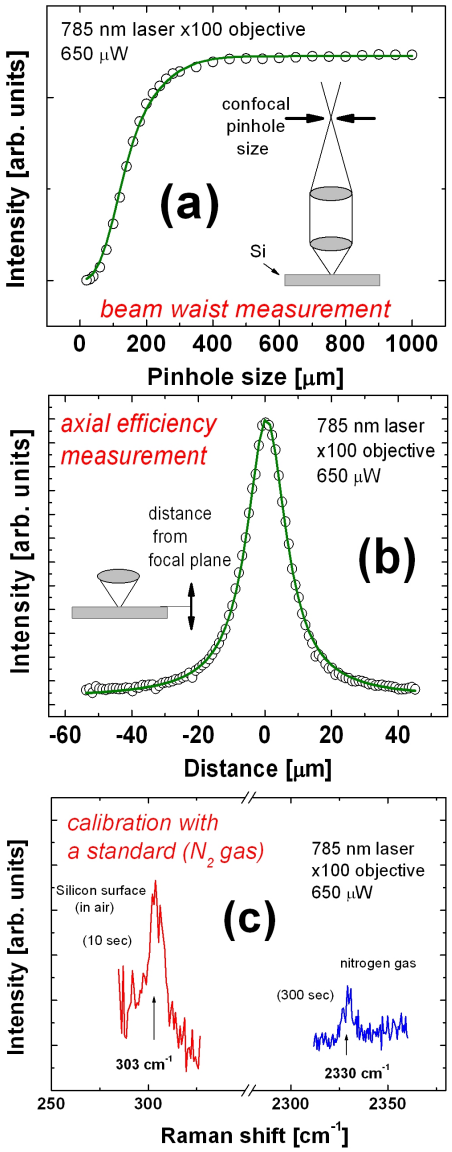

FIG. S1: Characterization of the scattering volume of the microscope (see the supplementary information in Ref. 2 for an in-depth description of the procedure). The beam waist is measured in (*a*) by studying the pinhole size dependence of the intensity of the 520 cm^{-1} Raman peak of Si at the confocal plane (through the magnification of the collecting optics, which for our system is a factor of 56). The solid line shows the fit to the data following Ref. 2. In (*b*) the axial signal dependence is measured with the confocal pinhole fully opened, to define the *effective depth of focus*. This is done by measuring the signal for different positions of the sample with respect to the focal plane. The line in (b) is a guide to the eye; the actual confocal depth is calculated with Eq. S33 in Ref. 2. The data in (*b*) and the beam waist from (*a*) define the effective scattering volume [2]. In (*c*), a reference sample with a known Raman differential cross section (nitrogen gas) is measured in the scattering volume. The signal is then compared (with a normalization to account for the system response at different wavelengths) to the 303 cm^{-1} peak of Si to define an apparent cross section. This can then be used to quantify the differential cross sections of individual nanotubes from Ref. 1.

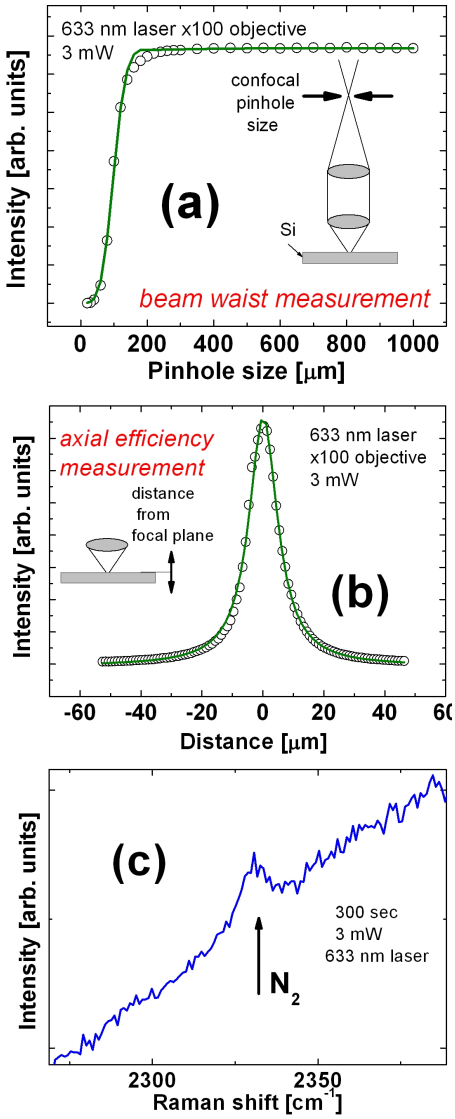

FIG. S2: (a) Beam waist and (b) axial efficiency characterizations of the scattering volume for the 633 nm laser with a ×100 objective (indexed matched to air). The combination of the results in (a) and (b) rendered a beam waist of $w_0 = 450\,\mathrm{nm}$, an effective depth of focus of $H_{\mathrm{eff}} = 16.5\,\mu\mathrm{m}$ (from Eq. S33 in Ref. 2), and an effective scattering volume V_{eff} of $5.25\,\mu\mathrm{m}^3$. (c) Nitrogen gas (in air) Raman signal at normal pressure and temperature. This signal is equivalent to an effective differential cross section of $1.6 \times 10^{-23}\,\mathrm{cm}^2/\mathrm{sr}$ and has been obtained with 300 sec integration time. The signal in (c) (normalized by the difference in integration times) serves as a basis to quantify the individual RBM's in Fig. 3 of the main text.

collecting optics, etc), we can focus the laser on a Si substrate (in air) and obtain the signal of the second-order (acoustic phonons) Raman peak of Si at $\sim 303\,\mathrm{cm}^{-1}$; this is also shown in Fig. S1(c). The ratio of integrated intensities with respect to the nitrogen signal allows us to define an *apparent* differential cross section per unit area

for this feature at a Si/air interface. Note that *this is not the differential cross section*, which in a solid is normally given for crystals as a differential cross section per unit cell (or per atom) [4, 5]. The apparent differential cross section per unit area, on the contrary, is simply a value to link the intensity of this peak to a known standard. For as long as we use the same laser (*i.e.* the same penetration depth) in another experiment, we can link the intensity of this feature in Si to a known standard through the definition of the apparent cross section per unit area. For the signal on the Si substrate we define:

$$I_{\mathrm{Si}}^{(1)} = \alpha\rho\tau \cdot \frac{d\Sigma}{d\Omega} \cdot A^{(1)} \tag{S2}$$

$$\Longrightarrow \quad \frac{d\Sigma}{d\Omega} = \frac{I_{\mathrm{Si}}^{(1)}}{I_{\mathrm{N_2}}} \cdot \frac{N}{A^{(1)}} \cdot \left(\frac{d\sigma}{d\Omega}\right)_{\mathrm{N_2}}^{785\,\mathrm{nm}}, \tag{S3}$$

where $d\Sigma/d\Omega$ is the apparent cross section per unit area of the Si substrate (for the $\sim 303\,\mathrm{cm}^{-1}$ mode), $A^{(1)}$ is the laser spot area in this experiment; and ρ, τ, and α have the same meaning as before. Note that $d\Sigma/d\Omega$ is obtained through a ratio of intensities measured with the same spectrometer and, accordingly, it becomes independent of ρ and (more importantly) of α. Note also that $d\Sigma/d\Omega$ is an intrinsic property of Si at this wavelength and it has units of sr^{-1} (because it is a cross section per unit area). Last, but not least, $d\Sigma/d\Omega$ needs to be corrected by the response of the system; this is necessary because the $2331\,\mathrm{cm}^{-1}$ mode of nitrogen is far from the $303\,\mathrm{cm}^{-1}$ mode of Si and (in the NIR in particular) the system response might not the same. Our system detects 3.35 times more at $303\,\mathrm{cm}^{-1}$ than $2330\,\mathrm{cm}^{-1}$ (with respect to a 785 nm excitation), as measured by comparison with a calibrated halogen lamp of known effective emission (black-body) temperature (2700 K). With all factors taken into account we find:

$$\frac{d\Sigma}{d\Omega} = 5.43 \times 10^{-14}\,\mathrm{sr}^{-1} \qquad \text{at } 785\,\mathrm{nm} \tag{S4}$$

We now have all the elements to link the signals of RBM's from individual nanotubes to a known standard in experiments performed by others. If the area of the laser spot in somebody else's experiment at 785 nm is known, and the $303\,\mathrm{cm}^{-1}$ Si signal is visible, we can always deduce what the equivalent differential cross section of the latter is, and relate this (through a simple intensity ratio) to the signal of the RBM's of nanotubes in the same spectrum.

Explicitly, knowing the area of the laser spot in Ref. 1 ($A^{(2)} \sim 1\,\mu\mathrm{m}^2$), the Si signal can be expressed as:

$$I_{\mathrm{Si}}^{(2)} = \alpha_2\rho_2\tau_2 \cdot \frac{d\Sigma}{d\Omega} \cdot A^{(2)}, \tag{S5}$$

where ρ_2, τ_2, and α_2 are again the power density, integration time and internal system response (for this new experiment, which could be done in a completely different spectrometer), $A^{(2)}$ is the new laser spot area and $d\Sigma/d\Omega$ is the (intrinsic) cross section per unit area of the $303\,\mathrm{cm}^{-1}$ Si signal coming from our calibration in Eq. S3. On the other hand, the signal of a RBM of a single carbon nanotube in the same spectrum will be given by:

$$I_{\mathrm{SCNT}}^{\mathrm{RBM}} = \alpha_2\rho_2\tau_2 \cdot \left(\frac{d\sigma}{d\Omega}\right)_{\mathrm{RBM's}}^{785\,\mathrm{nm}}, \tag{S6}$$

from where (taking the intensity ratio with Eq. S5, and replacing the expression for $d\Sigma/d\Omega$) we obtain:

$$\left(\frac{d\sigma}{d\Omega}\right)_{\mathrm{RBM's}}^{785\,\mathrm{nm}} = \frac{I_{\mathrm{SWNT}}^{\mathrm{RBM}}}{I_{\mathrm{Si}}^{(2)}} \cdot \frac{d\Sigma}{d\Omega} \cdot A^{(2)}. \tag{S7}$$

From Ref. 1 a value of ($A^{(2)} \sim 1\,\mu\mathrm{m}^2$) was assumed, while $I_{\mathrm{SWNT}}^{\mathrm{RBM}}$ and $I_{\mathrm{Si}}^{(2)}$ were estimated from Fig. 2 of Ref. 1 (reproduced in Fig. 1 of the main text). The resulting RBM cross-sections are summarized in Table I of the main text.

SECTION S2: CARBON NANOTUBE AND SAMPLE PREPARATION

Vertically aligned ^{13}C single-wall nanotubes were synthesized at 850 °C using ethanol as a carbon source in a no-flow condition [6, 7]. This sample has been synthesized for a different purpose, but it turned out to be ideal for the determination of differential cross sections of single nanotubes. The isotopic substitution from ^{12}C to ^{13}C is of no consequence for this experiment, except for the fact that RBM frequencies appear at slightly smaller wavelengths. For the synthesis, Co/Mo binary metal particles were formed on a quartz substrate as the catalyst using dip-coating. The substrate was then annealed in air at 400 °C for 5 min before being heated to 850 °C under a 300 sccm (standard cubic centimeters per minute) Ar/H_2 flow (3% H_2, Ar balance) at a pressure of 40 kPa. Upon reaching the growth temperature, the chamber was evacuated. 1.3 kPa of ethanol was then introduced into the chamber to start the SWNT growth. To prepare a solution sample, the obtained SWNT film was scratched off the quartz and dispersed in D_2O with 0.5 wt% sodium dodecylbenzene sulfonate (NaDDBS) by a bath sonication for 30 min, followed by a horn sonication with an ultrasonic processor (Hielscher GmbH, UP-400S with H3/Micro-Tip 3) for 15 h at a power flux level of $\sim$300 W/cm^2. The solution is then dried on a clean Si wafer and subsequently dip-washed several times with both distilled water and ethanol (separately). The wafers look "almost clean" to the bare eye after repeated washing, but a closer look with Scanning Electron Microscopy (SEM) reveals isolated clusters of nanotubes strongly attached to the surface.

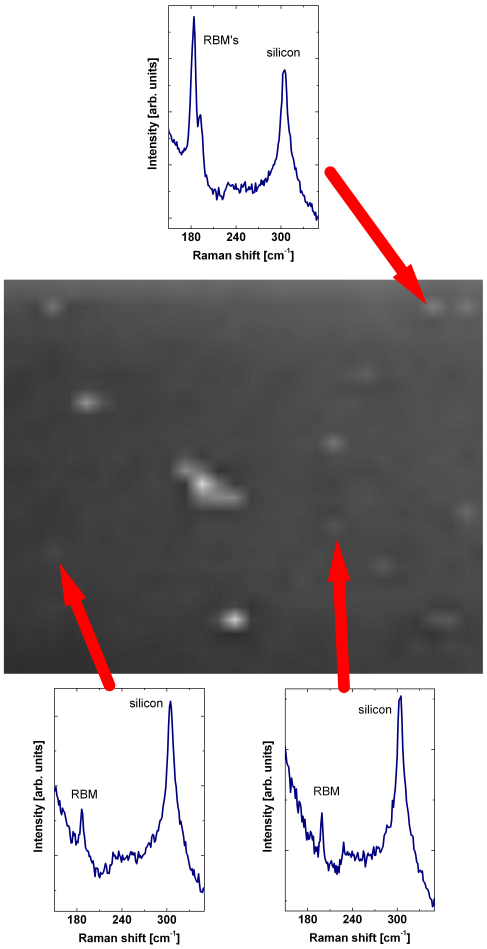

FIG. S3: A 40×40 (1μm spacing) Raman map at 633 nm (3 mW) and 10 sec integration time (see the main paper for further details on the experimental conditions). The map shows –in a black-white color scale– the integrated intensity of the spectrum in the RBM-fingerprint region ($\sim 150 - 220\,\mathrm{cm}^{-1}$). The "large" white islands represent regions with multiple (possibly entangled) tubes. Only the weakest isolated points in the map produce signals where only one RBM is present in the spectrum. A few of these isolated spots show sometimes evidence for more than one type of tube at the spot position. The spectrum at the top, for example, shows a case with two RBM's.

SECTION S3: RAMAN MAPS

Raman maps were taken (under the experimental conditions reported in the main paper) on 40×40 grids with points separated by 1 μm. Here we show an example of one of these maps. Most of the time, the signal is simply the spectrum of the substrate (Si). But in a few sparse places, signals with peaks in the fingerprint region of RBM's can be observed. In Fig. S3 we show a map where the integrated intensity in the RBM-region ($\sim 150 - 220\,\mathrm{cm}^{-1}$) is plotted as a function of position.

Several places in the map show evidence of "cluttering" of tubes with many different contributions from different RBM's. Only isolated (weaker) spots show evidence of signals coming from single tubes. Every so often it is possible to find isolated spots with signals from more than one tube (an example of which is shown at the top of Fig. S3). Two examples (at the bottom of Fig. S3) of single nanotube Raman signals with different RBM's are explicitly shown in the map. Only cases where the spectral purity of the RBM region is good enough to assign it to a single tube are used in the statistics of the differential cross sections shown in the paper (Fig. 4 of the main paper).

[1] A. Jorio, R. Saito, J. H. Hafner, C. M. Lieber, M. Hunter, T. McClure, G. Dresselhaus, and M. S. Dresselhaus, Phys. Rev. Lett. **86**, 1118 (2001).

[2] E. C. Le Ru, E. Blackie, M. Meyer, and P. G. Etchegoin, J. Chem. Phys. C **111**, 13794 (2007).

[3] E. C. Le Ru and P. G. Etchegoin, *Principles of Surface Enhanced Raman Spectroscopy and Related Plasmonic Effects* (Elsevier, Amsterdam, 2009).

[4] P. Y. Yu and M. Cardona, *Fundamentals of semiconductors: physics and materials properties* (Springer, Berlin, 2004).

[5] W. Hayes and R. Loudon, *Scattering of light by crystals* (Wiley, New York, 1975).

[6] Y. Murakami, S. Chiashi, Y. Miyauchi, M. Hu, M. Ogura, T. Okubo, and S. Maruyama, Chem. Phys. Lett. **385**, 298 (2004).

[7] R. Xiang, Z. Zhang, K. Ogura, J. Okawa, E. Einarsson, Y. Miyauchi, J. Shiomi, and S. Maruyama, Jpn. J. Appl. Phys. **47**, 1971 (2008).